RASĀYAN *J. Chem.*
Vol. 19 | No. 1 | 393-399 | January-March | 2026
ISSN: 0974-1496 | e-ISSN: 0976-0083 | CODEN: RJCABP
http://www.rasayanjournal.com
http://www.rasayanjournal.co.in

ENHANCEMENT OF CORROSION RESISTANCE ON ZINC ANODE IN ALKALINE ENVIRONMENT THROUGH ELECTROPLATING METHODS

Priya Garg[1], Sudhish K. Shukla[1,✉]and Pradeep K. Varshney[2]
[1]Department of Sciences, Manav Rachna University, Faridabad, India
[2]Swami Rama Himalayan University, Dehradun, India
✉Corresponding author: sudhish.shukla@gmail.com

ABSTRACT

This research explored the electrochemical corrosion behavior of tin- and copper-coated zinc anodes in an alkaline environment (2M-10M KOH), aiming to boost zinc-air battery efficiency.The electrochemical properties of coated zinc anodes were characterized using Electrochemical Impedance Spectroscopy, yielding detailed information on their impedance behavior and protective efficacy during immersion. Further, scanning electron microscopy was employed to characterize the surface morphology. The experimental data distinctly highlighted the superiority of tin-electroplated zinc anodes in terms of protective characteristics, particularly when exposed to 7 M KOH alkaline solution, compared to other coating samples. The improved performance of the Sn-plated zinc anode is largely due to its notable resistance to stress corrosion cracking. Moreover, the tin coating provided a more efficient application process and substantially increased the mechanical strength of the zinc alloy in the alkaline electrolyte. As a result, tin-electroplated zinc emerges as a highly promising option for improving the durability and overall performance of zinc-air batteries.

Keywords: Zn–Air Battery, Dendrite Reduction, Coating Processes, Electrochemical Impedance Spectroscopy, Electroplating, Metal Air Batteries.

RASĀYAN *J. Chem.*, Vol. 19, No.1, 2026

INTRODUCTION

Metal-air batteries are emerging as a promising technology for energy storage due to their exceptional energy density, inherently lower material costs, and reduced environmental footprint.[1-3] Their operational principle revolves around the oxidative reaction of a metal anode and the reductive reaction of atmospheric oxygen at the cathode. MABs exhibit a significant theoretical energy density advantage over conventional lithium-ion batteries due to their unique operating mechanism.[4] Among numerous MAB chemistries, zinc-based systems have emerged as the most developed and suitable for both primary and secondary applications. Zinc air battery (ZAB) exhibits theoretical specific energies reaching up to 1352 Wh/kg (based on zinc mass) and theoretical energy densities of 9653 Wh/L (based on zinc volume). These figures significantly surpass those of current lithium-ion batteries (LIBs), which typically offer specific energies around 400 Wh/kg. This highlights ZABs as a promising next-generation battery technology. With affordable costs and inherent safety features, these batteries offer a promising solution for energy storage needs.[5-8] Despite their theoretical advantages, he development of ZABs faces several significant challenges. A primary concern is the rapid degradation of the zinc anode, which is largely attributed to its highly corrosive interaction with the alkaline electrolyte. This inherent corrosive behaviour necessitates the development and implementation of robust strategies aimed at significantly mitigating anode deterioration and enhancing its long-term stability. Moreover, the evolution of hydrogen gas [HER] during battery operation presents an additional critical challenge. This parasitic side reaction not only leads to significant energy loss, thereby reducing columbic efficiency, but also raises potential safety concerns due to gas accumulation, demanding meticulous attention in battery design and operation. Further, the development of a passivating oxide layer of ZnO on zinc surfaces contributes to the complexity of these issues. This insulating layer compromises the anodic voltage efficiency by increasing internal resistance and introducing considerable complexities into the overall battery operation, often leading to premature cell failure.[9-10] To fully harness the potential of ZABs, it is crucial to minimise

http://doi.org/10.31788/RJC.2026.1919530

parasitic electrolytic corrosion and hydrogen evolution, while simultaneously facilitating controlled, uniform, and highly reversible zinc dissolution and deposition during the charge and discharge cycles.[12–14,16] Achieving the widespread commercial viability and adoption of ZAB technology critically hinges on overcoming these fundamental material and electrochemical hurdles. However, the growing emphasis on environmental sustainability has, in turn, led to the diminished applicability of numerous traditional surface treatment techniques, emphasising the need for sustainable and innovative solutions.[11] The pursuit of effective corrosion-resistant coatings frequently involves either the strategic use of alloy-based treatment techniques or the exploration of alternative foundation materials to replace zinc. An optimal coating, in this context, is characterised by its superior corrosion resistance, robust adhesion to the substrate, inherent reliability, and exceptional uniformity, all of which are essential for long-term performance and durability of the battery.[15] This research explores the application of advanced deposition techniques to create thin films of copper[17] and tin[18-19]on electrode materials. These films may be further enhanced with strategic doping elements to produce a corrosion-resistant coating. Several methods exist for depositing Cu and Sn layers onto conductive surfaces.[21] Electroplating is a process that utilises electrolytic methods to apply Cu and Sn coatings to metal components.[22,32] The compatibility of Zn with Cu and Sn, combined with its natural electropositivity, makes metal-plated Zn a suitable option for enhancing corrosion resistance in alkaline solutions. Tin (Sn) emerges as the optimal choice due to its favourable Sn^{2+}/Sn redox potential (-0.14V) and substantial 451.6 mAh g^{-1} electron storage capacity.[20] Tin's stability is further enhanced by its high over potential for hydrogen evolution, making it suitable for electrochemical applications. It boasts an exceptionally high theoretical capacity per unit volume, surpassing that of numerous other metals. This inherent property enables the design of more compact batteries with enhanced energy storage capabilities. The relatively negative redox potential of tin facilitates efficient electron release during discharge, thereby enhancing cell voltage and improving electrochemical performance.

EXPERIMENTAL

Preparation of Electrode Material

The pure metallic zinc sheet (>99.2% purity) was purchased from Special Metals, Mumbai, of 0.2 mm thickness.

Electrodeposition Method for Coating on Zinc

To enhance the surface reactivity of the zinc (Zn) film, a pre-treatment process was employed using acetone to remove surface impurities. Initially, the zinc plates (99.2% purity, 1 cm × 1 cm × 0.2 mm dimensions) were treated with a dilute sulfuric acid solution to stimulate surface reactivity. The electroplating process was carried out at ambient temperature, applying 2-2.5 V for a duration of 15 minutes. The activated Zn substrate was immersed in a tin bath containing tin sulfate, sulfuric acid, and water. In this, Sn acts as anode whereas Zn serves as cathode, along with tin sulphate and water as the tin bath. After electroplating, the Zn film was subsequently rinsed with deionised water and dried under ambient conditions.[23-24]

Corrosion Rate Test

The gravimetric method, which precisely measures weight loss, is a widely recognized and reliable technique for evaluating corrosion inhibition efficiency.[25] To determine the corrosion rate, samples of regulated sizes were submerged. After immersion, the samples were washed, and their weights were compared before and after the exposure. The corrosion rate was computed based on the following formula:

$$\text{Corrosion Rate in}(\text{mg cm}^{-2}\ \text{h}^{-1}) = 87.6 \times [W/(D\ At)]$$

W= weight loss in milligram, D = density in (gram/cm^3), A = surface area in (cm^2), t = time in (hr)

Inhibition efficiency was calculated using the formula:

$$IE\% = (W_{blank} - W_{inhibitor})/ W_{blank}) \times 100$$

We also calculated the inhibition efficiency at various molar concentrations (2M, 4M, 6M, 7M, 8M, and 10M) of KOH and time intervals (30, 60, and 90 minutes) using the weight loss method. Notably, tin-coated zinc exhibited a significantly lower corrosion rate in a 7 M KOH solution after 60 minutes (Table-1).[26] Furthermore, the inhibition efficiency (IE) of tin-coated zinc attained its maximum value under these

optimal conditions. This enhanced inhibition efficiency is due to the synergistic effects of adsorption and the formation of a protective film on the metal surface, which collectively contribute to a robust blocking mechanism that impedes the corrosive process.[25] These findings strongly suggest that tin coating offers superior corrosion protection for zinc in alkaline environments.

Table-1: Corrosion Rate and Inhibition Efficiency of 7 M KOH over 60 Minutes

Metal Coating	Corrosion rate in 7 M KOH(60 min)		Inhibition efficiency	
	1st Set	2nd Set	1st Set	2nd Set
Zn	0.1207×10^{-3}	0.2300×10^{-3}	----	-----
Zn- Sn	0.0016×10^{-3}	0.0046×10^{-3}	75%	71%
Zn -Cu	0.0026×10^{-3}	0.2152×10^{-3}	60%	57%

RESULTS AND DISCUSSION

A comprehensive investigation was conducted to evaluate the electrochemical stability of electro-deposited Zn, Zn-Cu, and Zn-Sn electrodes. These experiments were conducted in a 7 M KOH alkaline solution at ambient temperature. To ensure reliable measurements, a three-electrode configuration was precisely designed and employed. This setup comprises an electroplated anode prepared by exposing a 1x1 cm^2 area through epoxy resin cladding, a saturated calomel electrode (SCE) serving as the auxiliary electrode, and a platinum wire as the reference electrode. All three electrodes were immersed to the same depth in the 7 M KOH solution. Electrochemical Impedance Spectroscopy (EIS), Cyclic Voltammetry (CV), and Linear Sweep Voltammetry (LSV) were performed consecutively. For EIS measurements, a frequency range of 0.01 Hz to 100 kHz was utilised at the initial open circuit potential (OCP), with a sine wave signal amplitude of 5 mV.

Cyclic Voltammetry (CV)

Cyclic voltammetry (CV) experiments were performed to investigate the electrochemical behaviour, oxidation-reduction reactions and redox potential processes of the electrodes in an alkaline environment. The resulting CV curves providevaluable insights into the corrosion resistance, electrochemical stability, and potential windows of the electrodes, enabling a comprehensive understanding of their electrochemical properties.[27]CV graph shown in Fig.-1 demonstrates the pronounced changes in the electrochemical characteristics of the zinc electrode after electroplating with copper (Cu) and tin (Sn) in a 7 M potassium hydroxide solution. The use of KOH as the electrolyte appeared to accelerate the redox reaction kinetics. All CVs were recorded at a scan rate of 50 mV/s within a potential range of 0.6 V to -1.8 V. As depicted in Figure 1b, the cyclic voltammograms for the bare Zn, Zn-Cu, and Zn-Sn electrodes consistently displayed well-defined anodic and cathodic peaks. Notably, the electrochemical measurements showed considerable differences in corrosion behaviour and electrochemical stability among the bare Zn, Zn-Cu, and Zn-Sn electrodes. The Zn-Sn electrode exhibited outstanding corrosion resistance and electrochemical stability, likely due to the formation of a protective tin oxide layer on its surface. In contrast, the Zn-Cu electrode displayed higher corrosion rates, which is plausibly attributed to galvanic coupling between zinc and copper, leading to preferential zinc corrosion. These findings emphasise the role of electrode composition for overall electrochemical performance and corrosion resistance. The Zn-Sn electrode exhibited a prominent cathodic peak at +3.257 V, corresponding to the reduction of the Sn coating. Upon reversing the sweep, a cathodic crossover was observed at a similar potential. The Sn coating on Zn likely forms a protective oxide layer, enhancing corrosion resistance. An anodic peak at -2.18 V was detected during the reverse scan, indicating the conversion of Sn hydroxides to Sn oxides during oxidation. Compared to bare Zn and Zn-Cu coated anodes, the Zn-Cu electrode showed significantly higher peak currents, indicating unique electrochemical behavior. The Zn-Cu electrode displayed a notable cathodic peak during the forward scan and distinct anodic peaks at +0.94 and -0.61 V. In contrast, the bare Zn electrode lacked a clear reduction peak, exhibiting only an anodic peak at +1.1 V during the reverse scan.[28]The Zn-Sn electrode exhibits a remarkably large peak separation between cathodic and anodic peaks, suggesting superior electrochemical stability in the 7 M KOH electrolyte (Table-2). This notable peak separation highlights the Zn-Sn electrode's enhanced resilience in alkaline conditions, demonstrating its potential for stable electrochemical performance.

Table-2: Representation of Peak Potential and Current Values for Various Coatings in 7M KOH

Metal	Potential (Epc) [V]	Current (ipc) [mA or μA]	Potential (Epa) [V]	Current (ipa) [mA or μA]	(ΔEp=Epa−Epc) [V]
Zn-Cu	-1.2	-0.5 mA	-0.2	0.5 mA	1
Zn-Sn	-1.3	-2.2 mA	-0.1	3.3 mA	1.2
Pure Zn	-1.5 (broad wave)	-0.4 μA	-0.1	1.1 μA	>1.0

Electrochemical Impedance Spectroscopy (EIS)

Electrochemical Impedance Spectroscopy (EIS) is a valuable tool for understanding electrochemical corrosion kinetics, especially in coating applications. To evaluate the corrosion resistance of bare Zn, Zn-Sn, and Zn-Cu anodes, EIS measurements were performed in 7 M KOH, spanning 0.01 Hz to 100 kHz.[30] The Bode and Nyquist plots (Fig.-1c and 2a) reveal complex impedance spectra with three distinct semicircles, suggesting multiple electrochemical processes at the electrode-electrolyte interface. At high frequencies, a capacitive semicircle appears, typically linked to double-layer capacitance at the interface. As frequency decreases, an inductive semicircle emerges, indicating a relaxation process tied to the corrosion reaction. At low frequencies, a second capacitive semicircle is seen, suggesting a diffusion-controlled corrosion process.[29] A crucial parameter derived from these plots is the diameter of the semicircular loops, which directly correlates with the anode's corrosion resistance; a larger loop diameter signifies enhanced corrosion resistance and improved durability. Conversely, smaller diameters indicate reduced corrosion resistance, emphasizing the need for optimized compositions or alternative coatings. Further, the high-frequency capacitive semicircle is attributed to the redox reaction of zinc ($Zn \rightarrow Zn^{2+}$), which governs the reaction rate. The inductive loop observed in the mid-frequency range is thought to arise from the deposition of intermediate species on the zinc film surface during electrochemical processes. Moreover, the secondary capacitive semicircle at lower frequencies is believed to be associated with the rapid resupply of reactants for the oxidation-reduction reaction. Notably, the Nyquist plots in Figure 1a reveal a significant increase in the capacitive loop diameter for both Zn-Cu and Zn-Sn anodes compared to pure Zn when measured in 7 M KOH. This increase directly translates to a rise in charge transfer resistance (Rt), consequently leading to a decrease in the corrosion rate. The high-frequency capacitive loop is primarily governed by the charge transfer resistance and the double-layer capacitance. The increased Rt value is likely due to the oxide film's ease of dispersion in high alkaline medium, exposing a fresh zinc surface.[31] The Nyquist plot effectively distinguishes the electrochemical performance of the three electrodes, revealing differences in charge transfer resistance and reaction kinetics. Notably, the Zn-Sn electrode exhibits the largest semicircle diameter, indicating the largest charge transfer resistance and superior corrosion resistance due to the passive oxide layer of tin forming over the surface of zinc.[31] Conversely, Zn-Cu shows the semicircle larger than bare zinc but smaller than Sn, which corresponds to the highest charge transfer resistance, implying slower reaction kinetics, but still this corrosion resistance is lower than Sn, which provides better passivating coating. In the case of bare Zn, the smaller loop diameter indicates a low Rt value and rapid corrosion, as bare zinc is highly active in an alkaline environment. According to the Bode plots in Fig.-1c, the Zn-Sn coated alloy exhibits the highest impedance at low frequencies, suggesting enhanced corrosion protection. In an alkaline medium, Sn forms a stable protective oxide layer that acts as a strong barrierthat significantly increases resistance to the flow of corrosion-causing ions. Therefore, the Bode and Nyquist plot of the EIS spectra provides valuable insights into corrosion kinetics, including charge transfer resistance, which confirms that the Sn coating provides the most protective coating against corrosion.

Surface Characterization

The surface morphology of zinc-based electrodes is significantly affected by the type of coating element and the KOH electrolyte concentration. The provided Scanning Electron Microscopy (SEM) images, presented as Fig.-2, illustrate these changes by showing the surface of Zn-Cu, Zn-Sn, and pure Zn films after 3600 seconds (1 hour) of immersion or treatment in 6 M, 7 M, and 8 M KOH solutions. Upon

observing the effect of the electrode material, the pure Zn films (Fig.-2c, 2f, 2i) consistently exhibit distinct crystalline structures, particularly prominent at higher KOH concentrations (7 M and 8 M).

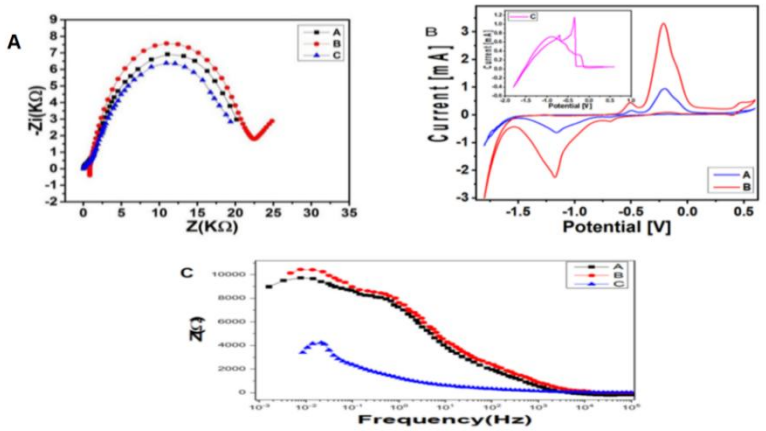

Fig.-1: A) The Nyquist Plot of (a) Zn-Cu, (b) Zn-Sn and (c) Bare Zn Electrode in 7 M KOH. B) The CV Curve of (a) Cu Coating, (b) Sn Coating and (c) bare Zn Electrode in 7 M KOH, Performed at a Scan Rate of 50 mV/sec. C) Bode Plot of (a) Zn-Cu, (b)Zn-Sn, and (c) Bare Zn Electrode in 7 M KOH Over a Range of 0.01 Hz to 100 kHz

These structures, described as needle-like or leaf-like (Fig.-2f) and larger flake-like structures (Fig.-2i), are characteristic of zinc oxide/hydroxide species formation, which are typically associated with passivation layers or discharge products in alkaline solutions.

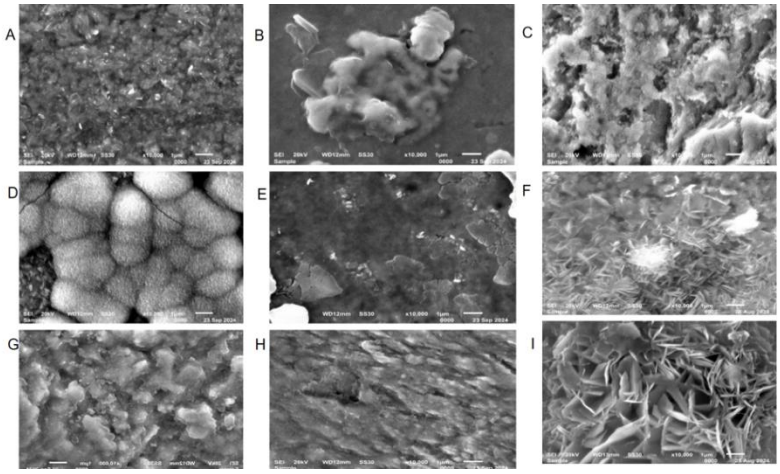

Fig.-2: SEM images of (a) Cu Coated, (b) Sn Coated, (c) Bare Zinc in 6 M KOH, (d) Cu Coated, (e) Sn Coated, (f) Bare Zinc in 7 M KOH, (g) Cu Coated, (h) Sn Coated, (i) Bare Zinc in 8 M KOH for 3600 Seconds

In contrast, the Zn-Cu films (Fig.-2a, 2d, 2g) display varied morphologies depending on the KOH concentration, ranging from a granular, porous surface in 6 M KOH (Fig.-2a) to a more defined, somewhat hexagonal or polyhedral structure in 7 M KOH (Fig.-2d), suggesting organized deposition or the formation of distinct inter-metallic phases. The Zn-Sn films (Figures 2b, 2e, 2h) tend to form more compact or flaky structures, with increasing concentration leading to a potentially smoother appearance. For instance, Fig.-2e shows a relatively flat surface with small particles, and Figure 2h depicts a smoother, more compacted film, indicating good adherence and a dense structure. The effect of KOH concentration is also evident across the electrode types. In 6 M KOH (Fig.-2a, 2b, 2c), the morphologies are generally less defined or more irregular, suggesting less uniform deposition or initial stages of surface evolution. The 7 M KOH concentration (Fig.-2d, 2e, 2f) appears to promote more distinct and often more organized features, with Zn-Cu forming a clear structured appearance (Fig.-2d), Zn-Sn appearing relatively flat (Fig.-2e), and pure Zn developing very prominent needle-like structures (Fig.-2f). At 8 M KOH (Fig.-2g, 2h, 2i), pure Zn continues to show well-defined crystalline products, potentially larger than those in 7 M KOH, while Zn-Sn appears smoother and more compacted. These changes in morphology with increasing

concentration are likely due to alterations in the solubility of zincate species and the kinetics of oxide/hydroxide formation. In conclusion, the SEM images provide crucial visual evidence that the surface morphology of zinc-based electrodes is significantly influenced by both the alloying element and the concentration of the KOH electrolyte. Pure Zn consistently forms distinct crystalline passivation layers, while Zn-Sn tends towards more compact films, and Zn-Cu exhibits varied structured appearances.

CONCLUSION

Electrodeposition is a versatile and efficient technique for surface modification. This study explored the use of electro-deposition to create copper Cu and tin Sn coatings on zinc film surfaces. The fundamental goal was to develop high-performance anodes for ZAB applications, leveraging the principle that electroplating can generate active sites to improve material efficiency and corrosion resistance in alkaline environments. The electrochemical performance of both Sn- and Cu-electroplated zinc anodes was rigorously evaluated in potassium hydroxide (KOH) solutions, ranging in concentration from 2M to 10M. A key focus was their suitability for high-performance applications. The findings reveal that the Sn-electroplated zinc anode demonstrates exceptional characteristics. It exhibits outstanding discharge capabilities, signifying efficient current delivery, and superior anodic efficiencies, suggesting high utilisation of the zinc material during electrochemical reactions. Moreover, this anode shows remarkable electrochemical stability, pointing to its potential for durable, long-term operation. These results suggest that Sn-electroplated zinc anode is a highly promising candidate for ZAB applications. Its unique combination of enhanced performance, improved durability, and cost-effectiveness represents a significant advancement in anode technology.

ACKNOWLEDGMENTS

The authors thank the University of Delhi for providing support in the characterisation of SEM and also for providing a workstation for EIS and cyclic voltammetry observation.

CONFLICT OF INTERESTS

The authors declare that there is no conflict of interest.

AUTHOR CONTRIBUTIONS

The present work is related to *SDG-9: Industry, Innovation and Infrastructure.* All the authors contributed significantly to this manuscript, participated in reviewing/editing, and approved the final draft for publication. The research profile of the authors can be verified from their ORCID ids, given below:

Priya Garg http://orchid.org/0009-0009-9495-4481
Sudish Kr. Shukla https://orcid.org/0000-0003-1867-396X
Pradeep K. Varshney http://orchid.org/0000-0003-4360-1204

Cite this article as: P. Garg *et al.*, *Rasayan J. Chem.*, 19(1), 393-399(2026), https://doi.org/10.31788/RJC.2026.1919530.

REFERENCES

1. H. Jiang, J. Gu, X. Zheng, M. Liu, X. Qiu, L. Wang, W. Li, Z. Chen, X. Ji, J. Li, *Energy Environmental Science,* **12**, 322(2019), https://doi.org/10.1039/C8EE03276A
2. H. Jiang, Y. Liu, W. Li, J. Li, *Small* **14**,1703739(2018), https://doi.org/10.1002/smll.201703739
3. X. Han, X. Li, J. White, C. Zhong, Y. Deng, W. Hu, T. Ma, *Advanced Energy Materials,* **8,** 1801396 (2018), https://doi.org/10.1002/aenm.201801396
4. H. F. Wang, Q. Xu, *Matter* **1**, 565(2019), https://doi.org/10.1016/j.matt.2019.05.008
5. Y. Li, H. Dai, *Chemical Society Reviews,* **43**, 5257(2014), https://doi.org/10.1039/C4CS00015C
6. J. Wang, Y. Li, X. Sun, *Nano Energy,* **2**, 443(2013), https://doi.org/10.1016/j.nanoen.2012.11.014
7. Y. Li, J. Fu, C. Zhong, T. Wu, Z. Chen, W. Hu, K. Amine, J. Lu, *Advanced Energy Materials,* **9**, 1802605(2019), https://doi.org/10.1002/aenm.201802605

8. V. Caramia, B. Bozzini, *Materials for Renewable and Sustainable Energy,* **3**, 28(2014), https://doi.org/10.1007/s40243-014-0028-3
9. L. Fan, H. Lu, J. Leng, *Electrochimica Acta,* **165**, 22(2015), https://doi.org/10.1016/j.electacta.2015.03.002
10. Y. Tang, L. Lu, H.W. Roesky, L. Wang, B. Huang, *Journal of Power Sources,* **138**, 313(2004), https://doi.org/10.1016/j.jpowsour.2004.06.043
11. V. S. Raja, *Frontiers in Metals and Alloys*, **1**, 894181(2022), https://doi.org/10.3389/ftmal.2022.894181
12. I. J. Park, S. R. Choi, J. G. Kim, *Journal of Power Sources*, **357**, 47(2017), https://doi.org/10.1016/j.jpowsour.2017.04.097
13. Q. Wang, H. Miao, Y. Xue, S. Sun, S. Li, Z. Liu, *RSC Advances,* **7**, 25838(2017), https://doi.org/10.1039/C7RA02918G
14. M. Jingling, W. Jiuba, Z. Hongxi, L. Quanan, *Journal of Power Sources,* **293**, 592(2015), https://doi.org/10.1016/j.jpowsour.2015.05.113
15. R. Bernasconi, L. Magagnin, *Surface Engineering*, **33**, 131(2017), https://doi.org/10.1080/02670844.2016.1175786
16. W. Wilhelmsen, T. Arnesen, O. Hasvold, N.J. Størkersen, *Electrochimica acta,* **36**, 79(1991) https://doi.org/10.1016/0013-4686(91)85182-7
17. T. Nagy, L. Nagy, Z. Erdélyi, E. Baradács, G. Deák, M. Zsuga, S. Kéki, *Batteries,* **8**, 212(2022), https://doi.org/10.3390/batteries8110212
18. L. Wu, F. Pei, Y. Zhang, Z. Long, Y. Liao, W. Lv, Y. Li, W. Zhang, H. Xu, Y. Huang, *ACS Energy Letters,* **9**, 5992, (2024), https://doi.org/10.1021/acsenergylett.4c02615
19. Y. Peng, C. Lai, M. Zhang, X. Liu, Y. Yin, Y. Li, Z. Wu, *Journal of Power Sources,* **526**, 231173(2022), https://doi.org/10.1016/j.jpowsour.2022.231173
20. S. G. Bratsch, *Journal of Physical and Chemical,* **18**, 1(1989), https://doi.org/10.1063/1.555839
21. H. Zhang, D. Xu, F. Yang, J. Xie, Q. Liu, D.J. Liu, M. Zhang, X. Lu, Y.S. Meng, *Joule,* **7**, 971(2023), https://doi.org/10.1016/j.joule.2023.04.011
22. D. Ahuja, S. Srivastava, P. K. Varshney, S. Srivastava, *Rasayan Journal of Chemistry*, **18**(1), 206(2025), http://doi.org/10.31788/RJC.2025.1819076
23. A. Tamilvanan, K. Balamurugan, T. Mohanraj Y. Admassu, *Journal of Nanomaterials* **2023**, 3431836(2023), https://doi.org/10.1155/2023/3431836
24. G. Panzeri, R. Dell'Oro, V. Trifiletti, J. Parravicini, M. Acciarri, S. Binetti, L. Magagnin, *Electrochemistry Communications,* **109**, 106580(2019), https://doi.org/10.1016/j.elecom.2019.106580
25. N. Anusuya, P. Sounthari, J. Saranya, K. Parameswari, S. Chitra, *Oriental Journal of Chemistry,* **31**,1741(2015), http://dx.doi.org/10.13005/ojc/310355
26. F. Malaret, Francisco, *Experimental results,* 3, e13(2022), https://doi.org/10.1017/exp.2022.5
27. P. T. Kissinger, W. R. Heineman, *Journal of Chemical Education,* **60**, 702(1983), https://doi.org/10.1021/ed060p702
28. A. U. Sardesai, V. N. Dhamu, A. Paul, S. Muthukumar, S. Prasad, *Micromachines*, **11**, 333(2020), https://doi.org/10.3390/mi11030333
29. A. M. Abdel-Gaber, E. Khamis, H. Abo-Eldahab, S. Adeel, *Materials Chemistry and Physics***, 109**, 297, (2008), https://doi.org/10.1016/j.matchemphys.2007.11.038
30. S. Hosseini, A. Abbasi, L. O. Uginet, N. Haustraete, S. Praserthdam, T. Yonezawa, S. Kheawhom, *Scientific reports,* **9**, 1,(2019), https://doi.org/10.1038/s41598-019-51412-5
31. J. Ren, J. Ma, J. Zhang, C. Fu, B. Sun, *Journal of Alloys and Compounds,* **808,** 151708(2019), https://doi.org/10.1016/j.jallcom.2019.151708
32. S. Srivastava, D. Ahuja, P.K. Varshney, *Journal of Energy Storage,* **76**, 109588(2024), https://doi.org/10.1016/j.est.2023.109588

[RJC-9530/2025]